Effect of the Cooling Rate on the Nucleation Kinetics of Poly(L-Lactic Acid) and Its Influence on Morphology

Manuel Salmerón Sánchez,*,†,‡ Vincent B. F. Mathot,§,|| Geert Vanden Poel,⊥ and José Luis Gómez Ribelles†,‡

Center for Biomaterials, Universidad Politécnica de Valencia, Camino de Vera s/n, 46022 Valencia, Spain, Centro de Investigación Príncipe Felipe, Autopista del Saler 16, 46013 Valencia, Spain, Laboratory for Macromolecular Structural Chemistry, Division of Molecular and Nanomaterials, Department of Chemistry, Katholieke Universiteit Leuven, Celestijnenlaan 200F, B-3001, Heverlee, Belgium, SciTe, Ridder Vosstraat 6, 6162 AX Geleen, The Netherlands, and DSM Research, Geleen, PO Box 18, 6160 MD Geleen, The Netherlands

Received June 7, 2007; Revised Manuscript Received July 27, 2007

ABSTRACT: Although the crystallization kinetics of PLLA is slow enough to allow one to obtain amorphous samples by cooling from the melt at moderate rates, surprisingly, at the same time, the formation of crystallization nuclei is difficult to avoid. Their amount depends on the cooling rate from the melt: the higher the cooling rate, the lower the amount of available nuclei after reaching the glass state. Cooling at controlled rates of 5−300 °C/min was performed by making use of a relatively new high-speed calorimetry technology, high-performance DSC (HPer DSC). Subsequent isothermal cold crystallization of amorphous PLLA, at different temperatures distributed across the bell-shaped crystal growth curve, was shown to depend on the rate at which the glass state was attained, reflecting the number of nuclei formed. However, (only) after complete cold crystallization, the DSC heating curves and the resulting morphology measured by optical microscopy and AFM were shown to be independent of the previous cooling rate into the glass, i.e., of the number of nuclei formed during the cooling process. In cases where the DSC heating curves subsequent to isothermal cold crystallization show two melting peaks, their origin, recrystallization, was clarified by heating at rates varying from 10 to 300 °C/min. The morphologies of the cold crystallized systems have been assessed by AFM and were correlated with the calorimetric results. Using HPer DSC, isothermal cold and hot crystallization at the same temperature has been studied successfully.

Introduction

Poly(L-lactic acid), PLLA, is a biocompatible and biodegradable polymer widely used in several biomedical applications.[1−4] PLLA is a promising material in regenerative medicine because it degrades through hydrolytic scission of the ester groups. The kinetics of bioresorption depends on the crystallinity and the semicrystalline morphology and, in general, it is faster in the amorphous domains (inter-/intra-spherulitic) than within the crystallites.[5,6]

The crystallization and melting behavior of PLLA has been extensively reported in the literature.[7−15] The crystallization rate of PLLA is quite slow, and it is possible to get an amorphous polymer by cooling from the melt at moderate rates.[10−13,16] Nevertheless, even if no crystal growth has taken place on cooling until the glass transition region is reached, the number of crystal nuclei is expected to be considerable because the nucleation rate increases with the supercooling,[17] the latter being the difference of the equilibrium melting temperature and the actual temperature. If the temperature is subsequently raised above the glass transition, in principle, crystal growth by "cold" crystallization can take place, as induced by the initial number of nuclei previously formed during the cooling step. Polymer crystallization might generally begin with the formation of mesomorphic entities acting as nuclei for the first crystallites.[i8] Further on in this article, the authors will use only the term nuclei. The number of nuclei present when, e.g., isothermal cold crystallization starts modulates the morphology of the system. This has been shown by increasing the initial number of nuclei by isothermal treatments just above and below the glass transition region in PLLA after first cooling, heating to a temperature above the glass transition, and then isothermal cold crystallization;[18] quite a number of spherulites grow simultaneously and yield a semicrystalline morphology very different from the one obtained by isothermal crystallization after a direct temperature jump from the melt. Such a direct temperature jump from the melt is named "hot" crystallization hereafter. In case of poly(ethylene terephthalate), PET, which also has slow crystallization kinetics, an analogous increase in the number of nuclei has been detected when isothermal treatments below the glass transition temperature are performed by the acceleration of the crystallization kinetics after increasing the temperature above T_g,[20−23] i.e., the physical aging process produces ordered domains able to act as crystallization germs.

As a work hypothesis, the rate of cooling from the melt also might affect the effective number of nuclei available to start the subsequent isothermal cold crystal growth process, i.e., the cooling rate from the melt is expected to tailor the nucleation kinetics. It has been suggested that the structure of glassy amorphous PET too is influenced by the cooling rate used to quench the samples from the melt and that differences in cooling rate cause changes in the cold crystallization rate above the glass transition as followed by measuring density, microhardness, and WAXD.[24,25]

* Author to whom correspondence should be addressed. E-mail: masalsan@fis.upv.es. Telephone: +34 96 3877275. Fax: +34 96 3877276.
† Center for Biomaterials, Universidad Politécnica de Valencia.
‡ Centro de Investigación Príncipe Felipe.
§ Department of Chemistry, Katholieke Universiteit Leuven.
|| SciTe.
⊥ DSM Research.

10.1021/ma0712706 CCC: $37.00
Published on Web 09/27/2007

This work investigates the nucleation processes that take place in PLLA on cooling at different-controlled rates from the melt. We make use of a relatively new high-speed calorimetry technology, high-performance DSC (HPer DSC), which represents a major step forward in high-speed calorimetry as compared to standard DSC.[26] This technique allows quantitative measurements at high, controlled cooling and heating rates of hundreds of degrees per minute of submilligram amounts of material. Use is made of this technique to study the influence of the cooling rate on the nucleation kinetics by cooling using a broad range of rates (5−500 °C/min) from the melt, resulting in amorphous PLLA with presumably different amounts of nuclei. Isothermal cold crystallization after cooling into the glass state at different rates and subsequent melting is investigated, also at different heating rates. The effect of the number of nuclei formed on cooling on the semicrystalline morphology of the isothermally cold crystallized samples was assessed by optical microscopy (OM) and atomic force microscopy (AFM).

Experimental Section

Materials. PLLA was synthesized by classical polycondensation procedures. The polymerization reactions were carried out as described elsewhere.[19] Briefly, a glass polymerization reactor equipped with a nitrogen flow-through inlet and a vacuum connection was placed in a temperature-controlled bath containing silicone oil. Polymerization was performed for 12−48 h in a nitrogen atmosphere within a temperature range of 100−150 °C. To remove residual monomers, chloroform and methanol were used as solvent and precipitant, respectively. The characteristic molar masses of the polymer, M_n and M_w, were 580 000 and 780 000 g/mol, respectively, as evaluated by gel permeation chromatography (Shimadzu, LC 10A, Japan) using polystyrenes as standards and chloroform as solvent.

HPer DSC Measurements. HPer DSC measurements were performed with a Perkin-Elmer Diamond HyperDSC.[27] This power-compensated DSC was selected to be used as HPer DSC because its furnace has low mass and small dimensions, ensuring a much faster heat transfer than in existing commercial heat-flux calorimeters. The small gap between the furnace and the aluminum cooling system, which is even more reduced by guard ring inserts, ensures effective cooling. The HPer DSC was cooled with a cryofill liquid nitrogen system, which ensures a very effective heat sink. Special attention was paid to the avoidance of water uptake by the gas tubes in the instrument, to the cooling of the instrument electronics, and to the prevention of water vapor condensation. As a gas atmosphere surrounding the reference and sample furnaces, a mixture of 10% helium and 90% neon was used. Temperature calibration is a critical issue in HPer DSC, and it was carefully performed according to ref 28. The symmetry of the DSC with respect to heat transfer in heating and cooling was checked using the smectic−nematic transition of 4-(4-pentyl-cyclohexyl)-benzoic acid-4-propyl-phenyl ester (HP-53), having a peak temperature at 120.5 °C.[29]

The thermal history of the samples was erased by heating from room temperature up to 200 °C and staying at this temperature for 3 min. Samples were cooled from the melt at different rates from 5 to 500 °C/min to produce a glassy polymer. The samples were subsequently taken to the cold crystallization temperature, and the crystallization process was then followed isothermally as a function of time. Subsequent melting after isothermal crystallization was measured at different heating rates. The sample masses have been conveniently reduced throughout to submilligram amounts within 0.85 ± 0.05 mg in order to minimize thermal lag. To promote optimal thermal contact between sample and sensor, 15 μm thick aluminum foils of approximately 0.5 × 1 cm^2 have been used to wrap the samples instead of using pans as sample containers. In all cases, an aluminum foil of the same dimensions was placed on the reference holder.

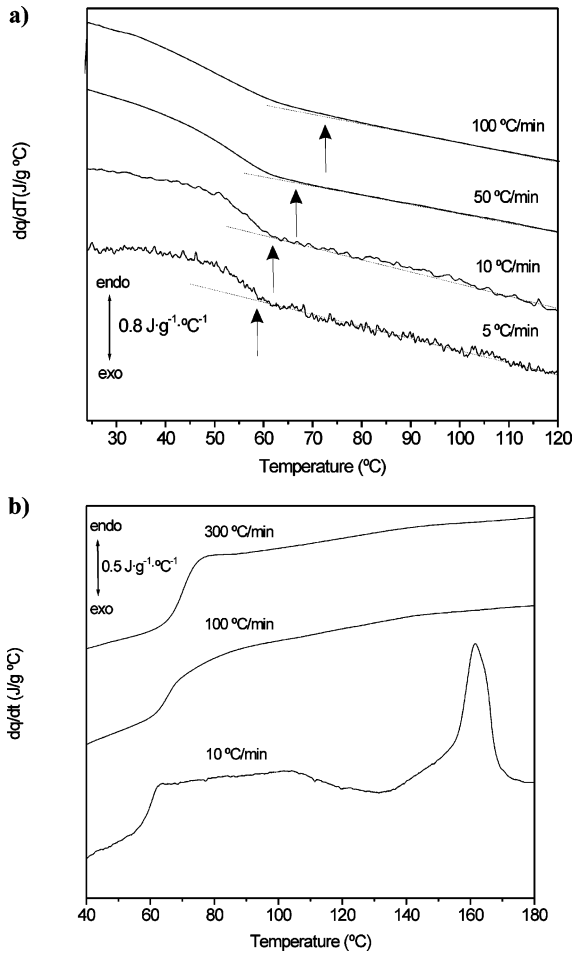

Figure 1. (a) DSC cooling curves at different rates from the melt. The arrows mark the shift of the onset of the glass transition to higher temperatures with increasing cooling rate. (b) DSC heating curves at different rates after cooling from the melt at 10 °C/min.

Atomic Force Microscopy and Optical Microscopy. Samples for AFM and OM were cast from a 1 m % solution in chloroform on circular microscopy slides. The thickness of the polymer layer was around 5 μm, estimated from the mass of the sample and the PLLA density. All thermal treatments were performed by using the Linkam THMS600 thermostatic plate of a Nikon Eclipse E600 optical microscope refrigerated with a flow of liquid nitrogen. The temperature calibration was performed with a benzoic acid standard.

The thermal treatments used started with annealing for 2 min at 200 °C, followed by cooling at the desired rate (10 or 90 °C/min) into the glass state (20 °C) and subsequent heating to the cold crystallization temperature, 110 °C. The crystallization process was followed by optical microscopy between crossed polarizers for 1 h. In a different set of thermal treatments, the crystallization process was stopped after 5 or 60 min and the sample subsequently cooled at 90 °C/min to room temperature, after which the surface of the sample was scanned by AFM at ambient conditions.

AFM images were recorded with a Nanoscope III from Digital Instruments. The microscope was placed on a vibration-protected table. An SSS-NCH Nanoworld cantilever, with a force constant of 42 N/m and a tip radius with a 5 nm curvature, was used. All samples were characterized using a set-point amplitude ratio of around 0.7.

Results

Dynamic Cooling and Heating. Figure 1a shows DSC curves as obtained on cooling from the melt at different rates after subtracting empty pan curves. T_g, defined as the temperature at which half of the total step in c_p (moving from above/below

Table 1. Glass Transition Temperatures, T_g, and Specific Heat Capacity Changes at T_g as a Function of Cooling Rate

cooling rate (°C/min)	T_g (°C)	Δc_p (J/g °C)
5	54.8	0.63
10	55.7	0.62
50	55.0	0.66
100	54.5	0.62

the glass transition temperature to below/above this temperature respectively) can be determined. Only the glass transition T_g appears at approximately 55 °C for every cooling and the onset of T_g increases with increasing cooling rate, as expected. However, also a broadening of the glass transition with increasing cooling rate is seen, which is why the temperature where half of the Δc_p jump (see Table 1) is realized is shifted toward lower temperatures, in contrast to what is expected. This phenomenon deserves further attention, but it is outside the scope of the present study. The specific heat capacity step at T_g, $\Delta c_p(T_g)$, remains approximately constant and equals 0.63 J/g•°C, see Table 1. This value is in agreement with the one reported for a fully amorphous PLA as obtained by quantitative thermal analysis.[30] No exothermal event is observed on cooling, which assures the amorphous character of all samples after cooling from the melt in the cooling rate range of this work (from 5 to 500 °C/min).

Figure 1b shows DSC heating curves at different rates after cooling from the melt into the glass state at 10 °C/min. It is clearly depicted that heating at 10 °C/min leads to cold crystallization, as the broad exothermal around approximately 130 °C shows. This event can be prevented by increasing the heating rate, and at rates of 100 °C/min and higher, only the glass transition is seen in Figure 1b. Thus, heating at such high rates clearly eliminates cold crystallization and as a result the heating curve reflects the preceding cooling scan, i.e., a reflection of an amorphous sample. These results show that it is possible, coming from the glass, to reach any temperature between T_g and the melt while keeping the sample in an amorphous state.

Isothermal Crystallization after Cooling at Different Rates. Parts a−c of Figure 2 show the isothermal cold crystallization DSC curves at different temperatures, subsequent to cooling from the melt into the glass state at different rates. The sample was cooled at a given rate (see Figures) from 200 to 20 °C and subsequently heated at 300 °C/min to the cold crystallization temperature. For such an extreme experiment, the use of a HPer DSC based on a small furnace in combination with power compensation is crucial because the high rate used avoids cold crystallization during heating before the desired temperature is reached. In addition, there is negligible "overshoot": the cold crystallization temperature is reached without passing it due to instrument inertia. This is realized by maintaining the high heating rate until a few degrees centigrade just below the programmed cold crystallization temperature and then slowing down of the scan rate. The isothermal heat flow rate caused by cold crystallization was then measured as a function of time for temperatures corresponding to the low-temperature and high-temperature sides of the "bell"-shaped crystal growth curve which for PLLA is located in between roughly 80 and 140 °C[7,8] and at its expected maximum at approximately 110 °C. The shapes of the DSC curves in Figures 2a−c are all seen to depend on the previous cooling rate. As the cooling rate decreases, a narrow peak appears at shorter times, followed by a broad one depicted in all the curves, which becomes independent of the preceding cooling rate for rates of 50−300 °C/min. The initial peak (at shorter times) has less

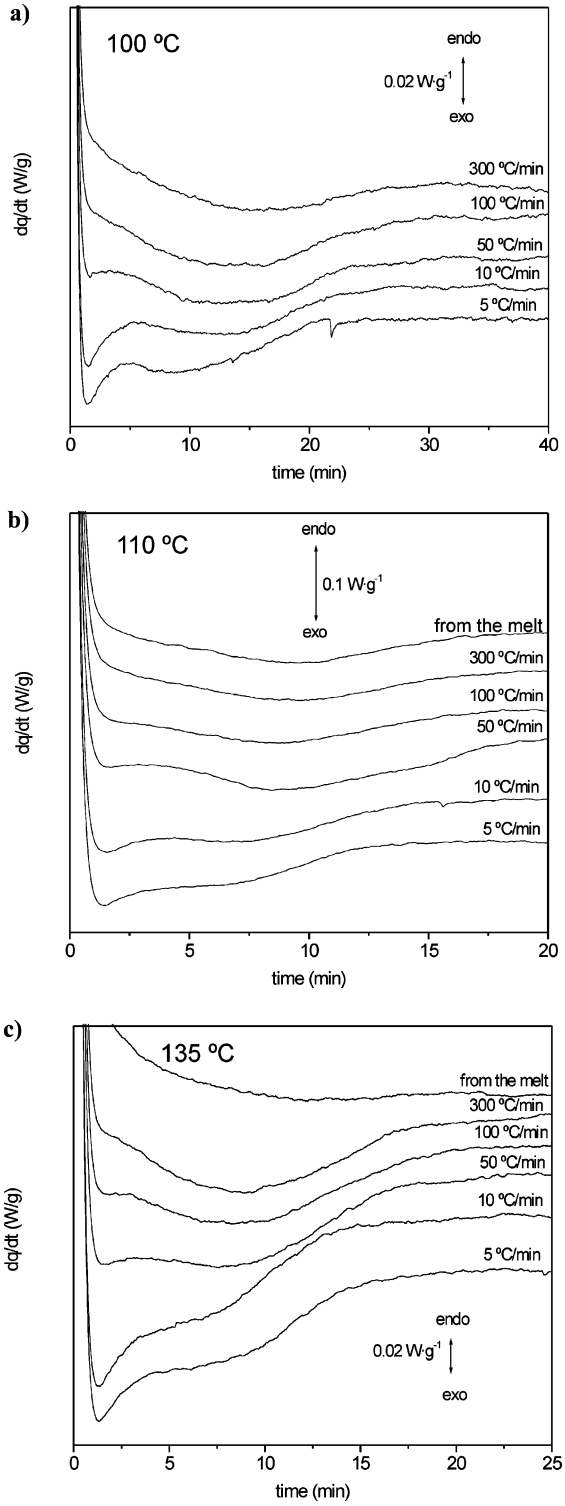

Figure 2. Isothermal cold crystallization at T_c for 60 min (only the time span is shown in which the curves show a changing heat flow rate signal) after heating from the glass state. The sample was previously cooled at different rates (shown at each curve) from the melt into the glass state. (a) T_c = 100 °C, (b) T_c = 110 °C, (c) T_c = 135 °C. In addition, isothermal hot crystallization curves after cooling directly from the melt at 100 °C/min are shown in (b) and (c).

intensity at 100 °C compared to 110 and 135 °C (note the scale bar). However, the minima (reflecting maximum heat flow rates) are located at approximately the same time (about 1−2 min; Figure 2a−c). Note that the same trends are found as a function of the cooling rate for any cold crystallization temperature (100, 110, 135 °C), independent of whether this temperature is located at the low-temperature side of the bell-shaped crystal growth

curve or at the high one. Note that there is hardly any difference between cold crystallization after the highest, preceding, cooling rates and hot crystallization in the case of crystallization temperatures at the low-temperature side of the crystal growth bell curve (Figure 2a,b). However, at 135 °C, which is located at the high-temperature side of the crystal growth bell curve, the kinetics of the isothermal hot crystallization is much slower than that for cold crystallization after the highest preceding cooling rate (Figure 2c).

After isothermal crystallization for 60 min, the samples were directly heated into the melt and the resulting DSC curves are shown in Figure 3a−c. Surprisingly, there is no effect of the cooling rate preceding the isothermal cold crystallization on the heating curves. The heating curves after crystallizing at 100 °C show two endothermic events, one at approximately 152 °C with a low-intensity and one at approximately 165 °C with a high-intensity, irrespective of the previous cooling rate. The heating curves after crystallizing at 110 °C also show two endotherms (the first one at approximately 158 °C and the second one, of lower intensity, at approximately 165 °C). In the case of cold crystallization at 135 °C, one peak is noticed in heating at approximately 166 °C. For "cold" crystallization at 100 and 110 °C, no differences are being observed compared with the heating curve obtained subsequent to "hot" crystallization of the sample at the same temperatures after direct cooling from the melt at 100 °C/min. This behavior changes when isothermal hot crystallization is performed at 135 °C, i.e., at the high-temperature side of the bell-shaped crystal growth curve: a melting endotherm with a smaller area is measured whose maximum is located at somewhat lower temperatures, see Figure 3c, i.e., a lower crystallinity is attained during the isothermal hot crystallization process (Figure 2c).

The fact that no effect of the preceding cooling rate is observed on the heating curves has to do with the time spent at the crystallization temperatures: the DSC heating curves in Figures 3a−c have been measured after completed crystallization; after 60 min at the crystallization temperatures of 100, 110, and 135 °C, respectively, see Figure 2a−c. To quantify the influence of the cooling rate and of the time spent at the isothermal cold crystallization temperatures on the subsequent melting process, the isothermal stage was stopped after different times and the subsequent DSC heating curves were measured. Parts a and b of Figure 4 show the evolution of the melting peaks with preceding cooling rate after cold crystallization at 100 °C for 1 and 5 min, respectively. The shapes of the curves change, resulting in melting enthalpies that vary considerably, see insets. It is clearly observed that the melting enthalpy depends strongly on preceding cooling rate and time of subsequent isothermal cold crystallization. The melting enthalpy, and therefore the crystallinity of PLLA too, decreases with increasing cooling rate, following a parabolic trend if a logarithmic scale is chosen for the *x*-axis. The melting enthalpy increases with increasing crystallization time (compare parts a and b of Figure 4) as expected.

Heating at Different Rates after Isothermal Cold Crystallization. The DSC heating curves at 10 °C/min after isothermal cold crystallization consist of double peaks whose origin seems not to be affected by the previous cooling rate, as seen in Figure 3. To clarify their origin(s), we make use of the possibility of controlled heating at different rates available in HPer DSC. Parts a and b of Figure 5 show DSC curves at different heating rates (10, 50, 100, and 300 °C/min) after isothermal cold crystallization at two different temperatures (100 and 110 °C, both for 1 h). The preceding cooling rate from the melt into the glass state

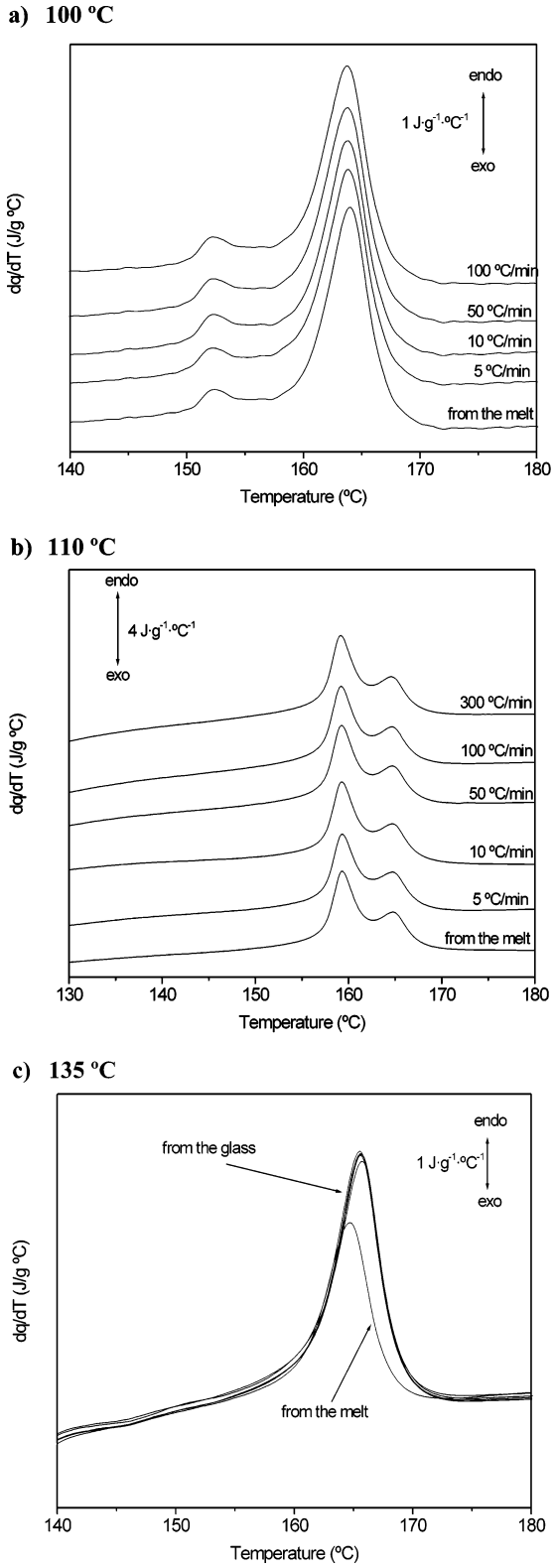

Figure 3. DSC heating curves at 10 °C/min after isothermal cold crystallization for 60 min at T_c [(a) $T_c = 100$ °C, (b) $T_c = 110$ °C, (c) $T_c = 135$ °C] coming from the glass state and from the melt. The cooling rate from the melt to the glass state is shown at each curve. Cooling directly from the melt was done at 100 °C/min.

was 100 °C/min. From these curves, it is clear that with increasing heating rate the low-temperature melting peak increases in intensity at the expense of the high-temperature melting peak. By that, the double melting peak behavior found at low rates (10 °C/min) transforms into a single one as the heating rate increases to 300 °C/min (Figure 5a) and 50 °C/

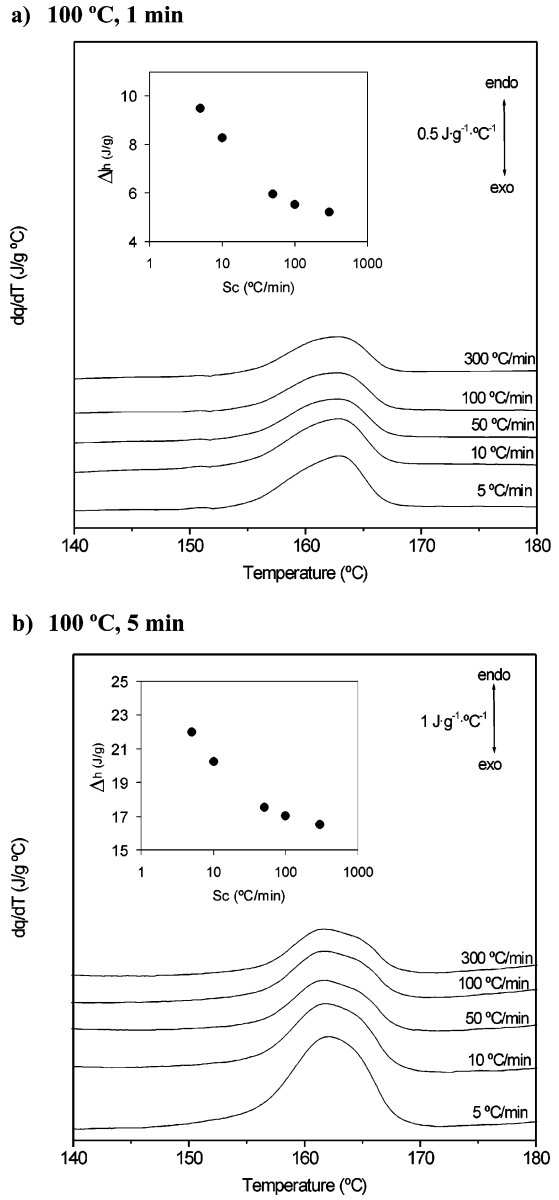

Figure 4. DSC heating curves at 10 °C/min after isothermal cold crystallization at 100 °C for t_c minutes coming from the glass. The cooling rate from the melt into the glass state is shown at each curve: (a) $t_c = 1$ min, (b) $t_c = 5$ min. Inset shows the melting enthalpy as a function of the scan rate in cooling, S_c, (on a logarithmic scale) from the melt to the glass state before the isothermal cold crystallization process.

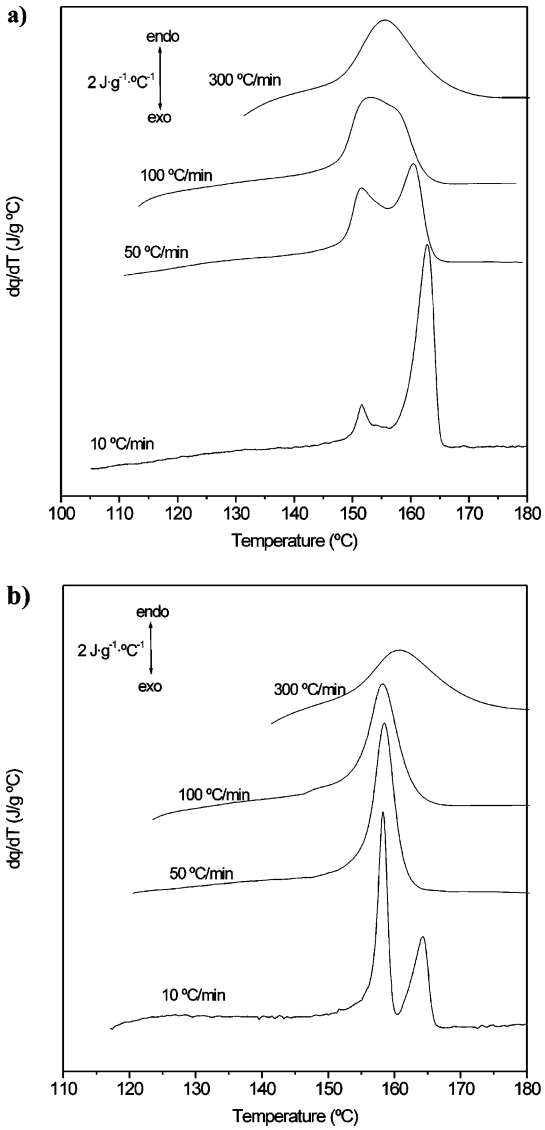

Figure 5. DSC heating curves at different rates after isothermal cold crystallization at T_c °C for 60 min. The heating rate is shown at each curve: (a) $T_c = 100$ °C, (b) $T_c = 110$ °C. The preceding cooling rate from the melt was 100 °C/min.

Table 2. Melting Peak Temperatures after Correction for Thermal Lag for the DSC Heating Curves in Figure 5a Following the Guidelines in Ref 28

heating rate (°C/min)	$T_{m,low}$ (°C)	$T_{m,high}$ (°C)
10	152.1	158.4
50	152.2	158.0
100	152.7	
300	152.0	

min (Figure 5b). At the same time it is seen that, as a result of an increasing thermal lag, the low-temperature peak shifts somewhat to higher temperatures by increasing the heating rate up to 100 °C/min and to an appreciable extent for heating at 300 °C/min.

The *usual first step* to correct for thermal lag is done by using metals like indium (by way of its onset temperature or extrapolated onset temperature) or using liquid crystals, by way of their peak temperatures as has been explained by Vanden Poel and Mathot.[28] In the present paper, this is done by *shifting of the whole DSC curve along the temperature axis* for the scan rate used, be it either in cooling, S_c, or in heating, S_h. Then, as *an optional second step* for correction of thermal lag, the *temperature of the maximum of a peak* can be corrected according to the guidelines in the same reference,[28] of which Table 2 shows the results: the temperature position of the low-temperature melting peak, after isothermal cold crystallization at 100 °C, agrees for all higher heating rates with that of the low-temperature melting peak of the double-peaked endotherm found at 10 °C/min.

It is the only way to compare the transition temperatures of samples having different masses and scanned at different rates. It is important to understand that correcting of the shape of the HPer DSC curve along the temperature axis is of no use because the thermal lag of each part of the curve depends in fact on the heat flow rate of the part itself, which is influenced by the amount of molecules taking part in the transition (like, e.g., crystallization, melting, etc.) and, in addition, the sample mass and applied rate. Therefore, up to now, no corrections have been made concerning the *shape* of the HPer DSC curves. A separate calibration in the cooling mode has not been done because, as

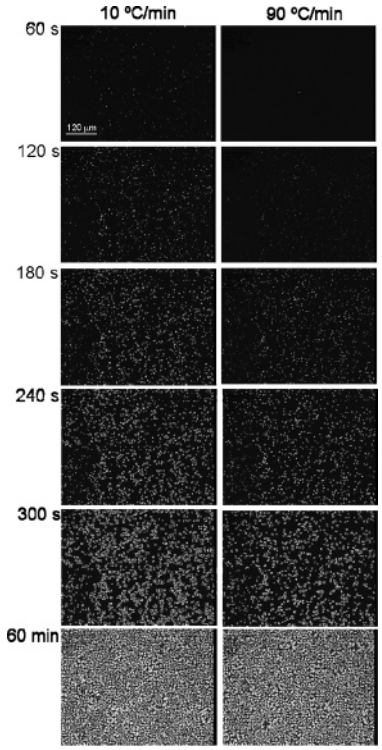

Figure 6. Isothermal (cold) crystallization process at 110 °C after cooling from the melt to the glass at two different rates (10 °C/min and 90 °C/min). The optical microscopy images show the number of simultaneously growing spherulites at different crystallization times (60 s, 120 s, 180 s, 240 s, 300 s, and 60 min). The scale bar is the same for all images.

remarked earlier, the symmetry of the DSC used with respect to the cooling and heating modes has been checked and found to be good.

Optical and Atomic Force Microscopy. Figure 6 shows the isothermal (cold) crystallization process at 110 °C after cooling from the melt to the glass at different rates (10 and 90 °C/min), as followed by optical microscopy. It is observed that the higher the cooling rate, the later the crystallization process starts. For the short times, the number of simultaneously growing spherulites (per unit volume) is higher in the sample crystallized at the lowest rate. Nevertheless, the morphology of the sample once the process is completed (i.e., after 60 min) is the same irrespective of the cooling rate.

Figure 7 shows AFM images after different thermal treatments. Parts a and b of Figure 7 show the spherulitic morphology of the system after stopping the isothermal cold crystallization process at 110 °C after 5 min subsequent to preceding cooling at (a) 10 and (b) 90 °C/min to room temperature. The number of spherulites (per unit volume) obviously depends on the cooling rate: cooling at 10 °C/min (Figure 7a) to the glass involves the formation of a much higher number of simultaneously growing spherulites during cold crystallization than cooling at 90 °C/min (Figure 7b) from the melt to the glass. Nevertheless, the average diameter of the spherulites is approximately the same after crystallizing for 5 min. Parts c and d of Figure 7 show that the final morphology of the system does not depend on the cooling rate (from the melt into the glass): approximately the same number of spherulites (per unit volume) is obtained with approximately similar diameters.

Discussion

PLLA crystallizes slowly enough so as to get the material amorphous by cooling at standard rates, e.g., 5 °C/min, from the melt. In such cases, only the glass transition step can be seen in the DSC cooling curve (Figure 1a). Besides, if the material is subsequently heated at high rates (e.g., 100 °C/min and higher), cold crystallization is also prevented and only the glass transition step appears in the DSC curves (Figure 1b). These experiments confirm the absence of any crystal formation during and after cooling from the melt using the procedure given, i.e., the material obtained after cooling from the melt, at any rate used in this work, is fully amorphous.

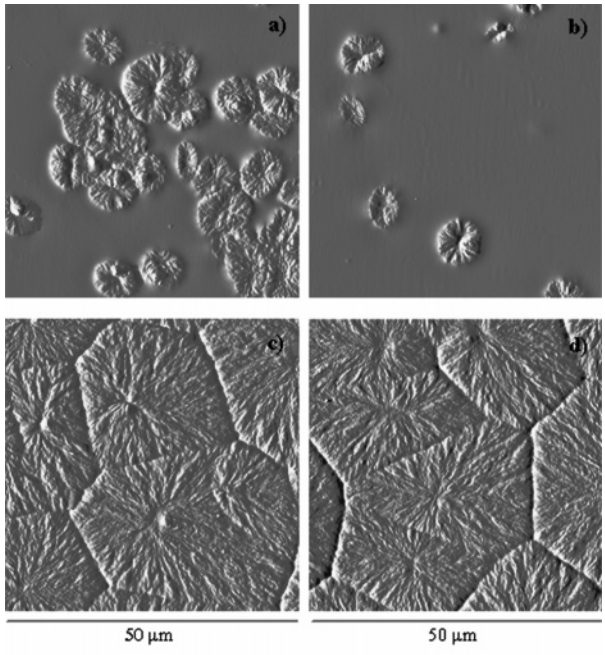

Figure 7. AFM amplitude images showing the spherulitic morphology after crystallizing at 110 °C for (a−b) 5 min, (c−d) 60 min. The samples were cooled at (a,c) 10 °C/min and (b,d) 90 °C/min from the melt into the glass before the isothermal cold crystallization process.

Nevertheless, even if no crystal growth process takes place on cooling, a certain number of nuclei is expected to be formed during this process whose number could depend on the cooling rate. The formation of a critical nucleus demands some time, which is determined by the rate at which the sample goes through the temperature interval[31] in which the formation of nuclei is thermodynamically possible, and thus the scan rate could influence the number of nuclei formed before the glass state is reached where nucleation is frozen in. If the sample is subsequently taken from the glass state to a temperature at which crystal growth can take place, the number of growing crystals then depends on the number of existing nuclei and, consequently, the isothermal cold crystallization kinetics could depend on the rate at which the glass state was reached coming from the melt, i.e., on the number of nuclei previously formed during the cooling process. Figure 2 shows that indeed the preceding cooling rate influences the isothermal crystallization rate: a sharp exothermal peak at relatively short times appears for low cooling rates that tend to vanish as the cooling rate increases, followed by a broader exothermal peak at relatively longer times. As the intensity of the short-time peak rapidly vanishes as the cooling rate at which the glass was formed increases, this peak is ascribed to crystal growth starting from nuclei already existing at the beginning of isothermal crystallization. In contrast, the long-time peak seems to be independent of the preceding cooling rate, and it can be ascribed to the growth of the crystallites from nuclei formed at the isothermal crystallization temperature. In conclusion, these features suggest the formation of less and less nuclei in the material as the preceding cooling rate increases.

This interesting phenomenon is observed at both sides of the bell-shaped crystal growth curve (Figure 2a,c) as well at its maximum, expected to be located somewhere around 110 °C (Figure 2b). As expected, the final crystallinity (as based on the melting enthalpy) and therefore the amount of crystallized material depends on the crystallization temperature: its value from cold crystallization at 110 °C is higher than that after isothermal crystallization at 100 °C and slightly higher than the value for 135 °C. This trend is found irrespective of the previous cooling rate.

Most intriguing is that heating after isothermal cold crystallization for *long-enough times* (long enough means in the present case 60 min, which is longer than the time needed for complete isothermal crystallization to take place, by which the heat flow rate does not change much anymore) gives rise to DSC heating curves that do not depend anymore on the previous thermal history, as can be learned from Figure 3a−c, except for the influence of temperature of isothermal cold crystallization. This suggests that a certain number of nuclei must have become active during the isothermal stay by athermal nucleation, leading to cold crystallization, which process obviously wipes out the initial nuclei density differences due to the preceding cooling at different rates. Moreover, it has become evident that the growth rate is slow compared with the nucleation rate. Two experimental facts support this argument. First, the presence of the long-time exothermal peak in the cold crystallization experiments does not depend on the preceding cooling rate (Figure 2a−c) and must be ascribed to the crystallization from nuclei that became active during the isothermal stage. Second, this is in line with the fact that the same spherulite morphology, independently of the preceding cooling rate, is reached in the material after long-enough times as is clearly depicted by OM and AFM (Figures 6, 7c,d): even though during short-ime cold crystallization the kinetics of crystallization depends on the previous thermal history, if enough time is given to the system, all nuclei will become active in the end, and the history does not matter anymore. The number density and size of the spherulites is approximately the same after crystallizing isothermally for 1 h independently of the previous cooling rate. As will be obvious from Figure 2a−c, any possible initial difference in the nucleation kinetics due to the preceding cooling rate will only be noticeable in the DSC results after cold crystallization for *short times*, and the same holds for the OM and AFM, which is confirmed by the results shown in Figures 6 and 7a−d.

Thus, the influence of the number of nuclei formed on preceding cooling on the isothermal cold crystallization kinetics can be observed in the heating scan only if the isothermal crystallization process is stopped after short crystallization times: that is on a minutes scale in the present case. Figure 4 shows the DSC curves after crystallizing for 1 and 5 min at 110 °C. The higher the cooling rate, the lower the melting enthalpy, which confirms the existence of a different number of nuclei and consequently a different number of crystallites. AFM and OM confirm the calorimetric results. Figure 6a,b shows that the number of spherulites growing at the same time is much higher the lower the cooling rate from the melt. Besides, the average size of the growing spherulites is approximately the same, which confirms it is determined by nuclei formed during the cooling stage from the melt to the glass.

Remarkably, see Figure 3c, the melting enthalpy after hot crystallization at 135 °C, located at the high-temperature side of the crystallization bell-shaped crystal growth curve (where crystal growth can take place but the nucleation rate is quite low), is much less compared to the melting enthalpy after cold crystallization at the same temperature due to fewer nuclei resulting from cooling directly from the melt, compared to nuclei becoming active by cooling into the glass. Samples were crystallized for 1 h at 135 °C before melting. This would mean that 1 h is not enough time for getting crystallization completed by hot crystallization due to the limited amount of nuclei and that, if more nuclei become active by coming from the glass, the crystallinity, after 1 h, is higher.

The double melting peak after isothermal cold crystallization for long-enough times (Figure 3a,b), independently of the previous thermal history, demands an explanation. The existence of several melting endotherms is a common feature in polymer systems.[32] It can have different origins, e.g., it might be caused by the existence of various crystal populations, differing in dimensions/perfections, or by the occurrence of melting−recrystallization−melting phenomena, i.e., reorganization by recrystallization processes are a symptom in the material as temperature increases. [Recrystallization is here defined in the classical way as the process where (part) of the crystallites melt (giving rise to a low-temperature endotherm melting peak), recrystallize (an exothermic signal, that either leads by superposition with the low-melting peak to a decrease in intensity and area of this melting peak or it becomes partly visible as a separate exotherm signal), and remelt (giving rise to a high-temperature endotherm melting peak). As such, recrystallization is one of the many ways reorganization can show up.] Possible recrystallization can be studied very well by HPer DSC by using combinations of cooling and heating at different, controlled rates.[26,33,34] Clearly, as seen Figure 5a,b, as the heating rate increases, the low-temperature melting peak increases at the expense of the high-temperature melting peak up to a scan rate at which the double melting behavior turns into a single one with its maximum, after proper correction for thermal lag, approximately at the temperature of the low-temperature melting peak, see Table 2. The behavior is qualitatively the same after crystallization at the different temperatures studied: 100 and 110 °C, see parts a and b of Figure 5, respectively. The low-temperature melting peak cannot be directly associated to the melting of the isothermally cold-crystallized material because most probably fast reorganization processes take place during heating from the (low) cold crystallization temperature to the low-temperature melting peak. In addition, because of the low-temperature cold crystallization, recrystallization is thermodynamically favored and, when heating is done at lower rates, kinetically possible. Increasing the heating rate prevents the recrystallization phenomenon and melting takes place in a single step. It is noteworthy that recrystallization is a relatively slow process for many polymer systems and can usually be suppressed effectively,[26,33,34] as is obvious in the present case of PLLA recrystallization.

Thus, recrystallization most probably is not the only type of reorganization taking place in PLLA during the experiments discussed. Even after preventing recrystallization phenomena, and after correcting for thermal lag, the single low-temperature melting peak resulting is to be expected to still be influenced by reorganization phenomena during heating. When no reorganization takes place, one expects melting to occur somewhat above the crystallization temperature because the dimensions of the crystallites have been increased compared to those of the nucleus as well as because of increased perfection. Because of the same reasons, as function of time at the crystallization temperature, melting will continue to shift to higher temperatures. Subsequently, during heating, the high mobility of the

molecules, also within crystallites,[35] at increasing temperatures facilitates reorganization of the crystallites into thermodynamically more stable ones. Such a kind of reorganization will be especially important in systems that are less stable with respect to dimensions and/or perfection, for instance, resulting from crystallization at low temperatures. Examples are crystallites obtained by quenching, by homogeneous of fractionated crystallization, or as in the present case, by cold crystallization. Most interesting is that extensive reorganization can result in melting temperatures even higher than those resulting from slow cooling or isothermal hot crystallization at high temperatures because reorganization during heating usually takes place at temperatures higher than the temperatures of hot crystallization, resulting in a higher mobility of the molecules involved. The relatively high heating rates of HPer DSC make it possible to prevent recrystallization, but most probably they are not high enough to prevent other reorganization processes during heating, causing the low-temperature melting peak (the one resulting after preventing recrystallization) to be much higher than expected. Thus, in the case of such fast reorganization, the direct connection between crystallization and melting behavior is expected to be (partially) lost. The proposition that in the present case reorganization is occurring is based on the emerging picture of reorganization during heating being a general phenomenon in case of polymers, and on the following specific observations for PLLA from the present research: first the still relatively high temperatures of the "single low-temperature melting peaks resulting after preventing recrystallization" compared to the cold crystallization temperatures (Figure 3a−c), and second, the melting peak after cold crystallization being situated at higher temperatures than after hot crystallization in case of crystallization at the high-temperature side of the bell-shaped crystal growth curve (Figure 3c). In the case of crystallization at the low-temperature side of the bell-shaped crystal growth curve, all melting events, including melting after hot crystallization, are expected to be shifted to higher temperatures because of reorganization. In conclusion, although it is evident that the faster the heating rate, the more reorganization will be hindered, probably a much higher heating rate is needed to fully prevent this kind of extensive reorganization effects in polymers, resulting in the determination of "real" melting events, meaning occurring at temperatures directly related to the thermal history of the sample without reorganization. Even so, heating with 10 000 °C/s of polyamide 6 using ultrafast chip calorimetry turned out to be not fast enough to completely avoid reorganization phenomena as discussed,[36] and whether it will work out for PLLA is not yet known.

Conclusions

HPer DSC allows cooling from the melt of PLLA in a broad, controlled cooling rate range by employing submilligram amounts of material. It is easy to obtain amorphous PLLA by cooling from the melt in a wide range of scan rates, e.g., at 5 °C/min and higher. Cold crystallization takes place on heating at low rates, which can be avoided by heating at rates of 100 °C/min and higher, by which the material keeps in the amorphous state during the whole procedure and only the glass transition is depicted in the corresponding DSC curves.

The cooling rate modulates the number of nuclei formed when the glass state is reached. Cooling at moderate rates result in high numbers of nuclei compared to samples cooled at higher rates. By that, faster subsequent cold crystallization kinetics, as detected by DSC, is provoked while these high numbers of nuclei also give rise to a higher number of spherulites growing simultaneously as assessed by OM and AFM.

For short times at the cold crystallization temperatures, the effect of different numbers of nuclei is reflected in the different enthalpies of melting resulting from subsequent DSC heating curves. For long-enough times, when cold crystallization is considered to be completed, however, neither the shape of the heating DSC curves nor the morphology by OM and AFM of the materials after crystallizing isothermally for 1 h do depend on the number of nuclei formed during the cooling step. This is explained by the formation of crystallization nuclei during the isothermal stage in such amount that these wipe out the initial nuclei difference due to the preceding cooling at different rates.

Melting after isothermal cold crystallization is shown to be a double process. Its nature was classified as caused by recrystallization by using the possibility of heating at high-controlled rates available by HPer DSC. Still the "single low-temperature melting peaks resulting after preventing recrystallization" are expected to be influenced by reorganization during heating.

Acknowledgment. M.S.S. acknowledges the financial support of the COST program through the COST−STSM-P12-01779 action and the Spanish Ministry of Science through the MAT2006-08120 project (including the FEDER financial support). We appreciate the discussions with Thijs Pijpers, SciTe/Katholieke Universiteit Leuven, Belgium, and the sample preparations for AFM by Jorge L. Escobar Ivirico, Technical University of Valencia.

References and Notes

(1) Södegard, A.; Stolt, M. *Prog. Polym. Sci.* **2002**, *27*, 1123.
(2) Thomson, R. C.; Wake, M. C.; Yaszemski, M. J.; Mikos, A. G. *Adv. Polym. Sci.* **1995**, *122*, 245.
(3) Kim, H. D.; Bae, E. H.; Kwon, I. C.; Pal, R. R.; Nam, J. D.; Lee, D. S. *Biomaterials* **2004**, *25*, 2319.
(4) Ma, Z.; Gao, C.; Gong, Y.; Shen, J. *Biomaterials* **2005**, *26*, 1253.
(5) Reeve, M.; McCarthy, S.; Downey, M.; Gross, R. *Macromolecules* **1994**, *27*, 825.
(6) MacDonald, R.; McCarthy, S.; Gross, R. *Macromolecules* **1996**, *29*, 7356.
(7) Salmerón Sánchez, M.; Gómez Ribelles, J. L.; Hernández Sánchez, F.; Mano, J. F. *Thermochim. Acta* **2005**, *430*, 201.
(8) Yasuniwa, M.; Tsubakihara, S.; Iura, K.; Ono, Y.; Dan, Y.; Takahashi, K. *Polymer* **2006**, *47*, 7554.
(9) Fujita, M.; Doi, Y. *Biomacromolecules* **2003**, *4*, 1301.
(10) Miyata, T.; Masuko, T. *Polymer* **1997**, *22*, 5515.
(11) Iannace, S.; Nicolais, L. *J Appl. Polym. Sci.* **1997**, *64*, 911.
(12) Di Lorenzo, M. L. *Eur. Polym. J.* **2005**, *41*, 569.
(13) Tsuji, H.; Tekuza, Y.; Saha, S. K.; Suzuki, M.; Itsuno, S. *Polymer* **2005**, *46*, 4917.
(14) Tsuji, H.; Miyase, T.; Tezuka, Y.; Saha, S. K. *Biomacromolecules* **2005**, *6*, 244.
(15) Xu, J.; Guo, B.-H.; Zhou, J.-J.; Li, L.; Wu, J.; Kowalczuk, M. *Polymer* **2005**, *46*, 9176.
(16) Wang, Y.; Gómez Ribelles, J. L.; Salmerón Sánchez, M.; Mano, J. F. *Macromolecules* **2005**, *38*, 4712.
(17) Vasoille, R.; Pérez, J. *Ann. Phys. (Paris)* **1985**, *10*, 10.
(18) Strobl, G. *Eur. Phys. J. E* **2000**, *3*, 165.
(19) Hernandez Sánchez, F.; Molina Mateo, J.; Romero Colomer, F. J.; Salmerón Sánchez, M.; Gómez Ribelles, J. L.; Mano, J. F. *Biomacromolecules* **2005**, *6*, 3283.
(20) Bove, L.; D'Aniello, C.; Gorrasi, G.; Guadagno, L.; Vittoria, V. *Polym. Bull.* **1997**, *38*, 579.
(21) McGonigle, E. A.; Daly, J. H.; Gallager, S.; Jenkins, S. D.; Liggat, J. J.; Olsson, I.; Pethrick, R. A. *Polymer* **1999**, *40*, 4977.
(22) Santa Cruz, C.; Baltá Calleja, F. J.; Zachmann, H. G.; Stribeck, N.; Asano, T. *J. Polym. Sci., Part B: Polym. Phys.* **1991**, *29*, 819.
(23) Fillon, B.; Lotz, B.; Thierry, A.; Wittmann, J. C. *J. Polym. Sci., Part B: Polym. Phys.* **1993**, *31*, 1395.
(24) Baltá Calleja, F. J.; García Gutierrez, M. C.; Rueda, D. R.; Piccarolo, S. *Polymer* **2000**, *41*, 4143.

(25) Kiflie, Z.; Piccarolo, S.; Brucato, V.; Baltá-Calleja, F. J. *Polymer* **2002**, *43*, 4487.
(26) Pijpers, T. F. J.; Mathot, V. B. F.; Goderis, B.; Scherrenberg, R. L.; van der Vegte, E. W. *Macromolecules* **2002**, *35*, 3601.
(27) After the high-performance DSC (HPer DSC) technique/method was developed[26] on the basis of a Perkin-Elmer Pyris 1 DSC, it was commercialized subsequently by Perkin-Elmer and trademarked as HyperDSC.
(28) Vanden Poel, G.; Mathot, V. B. F. *Thermochim. Acta* **2006**, *446*, 41.
(29) Neuenfeld, S.; Schick, C. *Thermochim. Acta* **2006**, *446*, 55.
(30) Pyda, M.; Bopp, R. C.; Wunderlich, B. *J. Chem. Thermodyn.* **2004**, *36*, 731.
(31) Debenedetti, P. G. *Metastable Liquids: Concepts and Principles*; Princeton University Press: Princeton, NJ, 1996.
(32) Wunderlich B, *Macromolecular Physics, Vol. 3: Crystal Melting*; New York: Academic Press; 1980; available by download as PDF from www.scite.eu.
(33) Mathot, V. B. F.; Vanden Poel, G.; Pijpers, T. F. J. *Am. Lab.* **2006**, *38*, 21−25. See also a recent webcast by V. B. F. Mathot, downloadable for free at www.hyperdsc.com and via www.scite.eu.
(34) Vanden Poel, G., Mathot, V. B. F. *Thermochim. Acta* **2007**, *461*, 107−121.
(35) Sumpter, B. G.; Noid, D. W.; Wunderlich, B. *J. Chem. Phys.* **1990**, *93*, 6875.
(36) Tol, R. T.; Minakov, A. A.; Adamovsky, S. A.; Mathot, V. B. F.; Schick, C. *Polymer* **2006**, *47*, 2172.

MA0712706